Intelligent robust adaptive attitude controller for small satellites

Intelligent robust adaptive attitude controller for small satellites

A Elrouby[1], H Hendy[2] and M Ashry[3]

[1]Optoelectronics Department, Military Technical College (MTC), Cairo, Egypt
[2]Space Research Center, Military Technical College (MTC), Cairo, Egypt
[3]Optoelectronics Department, Military Technical College (MTC), Cairo, Egypt

E-mail: asser.alrouby3@gmail.com

Abstract. This work addresses the issue of small-satellite attitude control. This satellite's Attitude-Control-System (ACS) is managed by an intelligent controller built on Adaptive Neuro-Fuzzy Inference System (ANFIS). ANFIS control approach is designed to improve the satellite's angular mobility along its axes. Two simulation scenarios have been tackled. In the first scenario, ACS system efficiency was evaluated and contrasted with ACS based on a PD controller optimized by a genetic-algorithm for the nonlinear system model and a Linear-Quadratic-Regulator (LQR) in the existence of input environmental disturbances. The simulation outcomes demonstrate that the proposed control technique successfully addresses the mobility issue of a small satellite. Inaccuracies in the satellite's parameters, torque noise brought on by the vibration of the actuators, and external disturbances were added in the second scenario. The proposed ANFIS controller has demonstrated robust, reliable performance for control of the ACS.

1. Introduction

Small satellite performance is improved thanks to developments in the shrinking of sensors, mechanical components, and processing hardware and software. The unique idea of collaborating satellites flying in a constellation opens up chances for a further expansion of the potential for offering both new services or functions and services similar to those already provided by huge and expensive spacecraft [1]. Proper stabilization and attitude control are essential for satellite application throughout all life cycle phases and are crucial for cooperation when flying in formation.

Both passive and active methods can provide mission control torques. Although passive attitude control doesn't use any power, it can only be used to dump unintended satellite motion brought on by outside disturbances [2]. Compared to passive techniques, active control offers greater control authority and permits the utilization of spacecraft actuators for rotating movements.

The two crucial parts of a satellite's attitude-control system (ACS) are the control method and the actuator. The actuators for satellite attitude control include reaction wheels (RWs), torque coils, control moment gyroscopes (CMG), magnetic rods, and thrusters. The main advantages of CMG over momentum and reaction wheels for agility movements are their significant torque amplification and capacity to store momentum. The biggest disadvantage of the thrusters is that they need fuel tanks, which use up power and space. Additionally, magnetic rods are unable

to give accurate pointing despite being lightweight. However, due to their pros in the sense of complexity, mass, volume, precision, and cost, reaction wheels are favored in small satellites [3].

Numerous satellite operation modes for various flight stages are outlined in [4]. The satellite has entered the final orbit and is prepared to carry out the mission in nominal mode. The RW serves as the primary actuator for small satellites in this mode.

A proportional derivative (PD) controller is utilized in [5, 6]. The controller in [5] is based on an inverse dynamics method, as opposed to the classical controller used in [6], to overcome the dependence of the controller's performance on the system inertia. In [6], several RW systems were used to determine which required the least control torque. For the ACS in nominal mode, the proportional integral derivative (PID) method is utilized [1]. A nanosatellite is controlled using the linear-quadratic regulator (LQR) optimum control technique in [4]. Contrary to [5, 6], which only considers stability, [1, 4] evaluated the controllers' abilities in satellite stabilization and reorientation. In [1, 4, 5, 6], the torque noise brought on by the RWs' vibration was not considered. Additionally, [1, 6] disregarded the impact of model uncertainty on controller performance. However, in [3], ACS built on a genetic algorithm (GA) adjusted gains PD controller and an LQR technique for the ACS were developed. Their performance was assessed in case of uncertainty and torque noise. As a result, both controllers have proven robustness and achieved better-pointing accuracy than in [1, 4, 5, 6].

The nominal mode is the subject of this paper. For the ACS, an adaptive neuro-fuzzy inference system (ANFIS) was established. Torque noise, model uncertainty, and external disturbances are all present throughout the testing of this controller. When performing stabilization and reorientation movements, the performance of ANFIS ACS is evaluated, and its results are contrasted with those of the controllers in [3].

This research covers the following: Attitude kinematic and dynamic equations are the primary focus of Section 2. In section 3, an overview of ANFIS is provided. Controller design was explained in section 4. The simulation findings are shown and analyzed in Section 5. Lastly, the conclusion can be found in the final section.

2. Mathematical representation

Valid principles for small satellites served as the foundation for satellite modeling. The targeted satellite lacks flexible appendages and has a rigid structure. Small spacecraft do not have fuel tanks to increase the payload mass relative to the platform mass. The products of inertia have all been set to zero in the Body Fixed Reference Frame (BFRF). On the principal axes of the satellite, three reaction wheels were employed as actuators. Using the above-mentioned assumptions, the satellite dynamics have been modeled, as in [3], by

$$\begin{aligned}
\dot{\omega}_{sx} &= \frac{J_{sy}-J_{sz}}{J_{sx}}\omega_{sy}\omega_{sz} + (\omega_{sz}\Omega_{ry} - \omega_{sy}\Omega_{rz} - \dot{\Omega}_{rx})\frac{J_w}{J_{sx}} + \frac{\tau_{dx}}{J_{sx}},\\
\dot{\omega}_{sy} &= \frac{J_{sz}-J_{sx}}{J_{sy}}\omega_{sx}\omega_{sz} + (\omega_{sx}\Omega_{rz} - \omega_{sz}\Omega_{rx} - \dot{\Omega}_{ry})\frac{J_w}{J_{sy}} + \frac{\tau_{dy}}{J_{sy}},\\
\dot{\omega}_{sz} &= \frac{J_{sx}-J_{sy}}{J_{sz}}\omega_{sx}\omega_{sy} + (\omega_{sy}\Omega_{rx} - \omega_{sx}\Omega_{ry} - \dot{\Omega}_{rz})\frac{J_w}{J_{sz}} + \frac{\tau_{dz}}{J_{sz}},
\end{aligned} \tag{1}$$

where ($\dot{\omega}_{sx}$, $\dot{\omega}_{sy}$, and $\dot{\omega}_{sz}$) are time derivatives of satellites' angular velocities seen from Earth Centered Inertial (ECI) frame mentioned in the BFRF frame (J_{sx}, J_{sy}, and J_{sz}) are the satellite's principal inertia moments, J_w is RW's inertia moment, (Ω_{rz}, Ω_{ry}, and Ω_{rx}) are the RWs' angular velocities about z, y, and x-axes of BFRF, ($\dot{\Omega}_{rz}$, $\dot{\Omega}_{ry}$, and $\dot{\Omega}_{rx}$) are the RWs' angular accelerations about z, y, and x-axes of BFRF, respectively, (τ_{dz}, τ_{dy}, and τ_{dx}) are the external perturbing torque components in the z, y, and x-axes of BFRF.

The representation of satellite kinematics is modeled as in [2] by

$$\begin{aligned}
\dot{\eta}_1 &= \frac{\omega_{sx}\eta_4 + \omega_{sy}\eta_3 - \omega_{sz}\eta_2}{2}, \\
\dot{\eta}_2 &= \frac{-\omega_{sx}\eta_3 + \omega_{sy}\eta_4 + \omega_{sz}\eta_1}{2}, \\
\dot{\eta}_3 &= \frac{\omega_{sx}\eta_2 - \omega_{sy}\eta_1 + \omega_{sz}\eta_4}{2}, \\
\dot{\eta}_4 &= \frac{-\omega_{sx}\eta_1 - \omega_{sy}\eta_2 - \omega_{sz}\eta_3}{2},
\end{aligned} \tag{2}$$

where ($\dot{\eta}_1$, $\dot{\eta}_2$, and $\dot{\eta}_3$) are the time derivatives of the satellite's quaternion's vector component, and $\dot{\eta}_4$ is the time derivative of the satellite's quaternion's scalar component.

2.1. Actuators modeling

Using the transfer function, each reaction wheel has been modeled as in [3], as

$$\frac{\dot{\Omega}_r(s)}{V_{ar}(s)} = \frac{sK_{to}}{(sJ_w + B_v)(sL_{ar} + R_{ar}) + K_{to}K_{em}}, \tag{3}$$

where $\dot{\Omega}_r(s)$ is the Laplace transform of the angular acceleration of the RW, $V_{ar}(s)$ is Laplace transform of armature voltage (L_{ar}, R_{ar}) are the armature circuit's inductance and resistance, B_v is the frictional constant of viscosity for the RW, K_{em} is the voltage constant, and K_{to} is the motor's torque constant.

2.2. Disturbances modeling

To mimic the attitude dynamics of the satellite, the disruptive torques (internal and external) impacting the satellite must be considered. Moveable mechanisms are typically the leading cause of disturbing internal torques. On the other hand, the satellite interacts with the space environment to create external perturbing torques, including gravity-gradient, magnetic, solar radiation pressure, and air drag disturbing torques. Environmental torques have been modeled in this work according to [3, 4].

3. ANFIS

Fuzzy and neural network approaches are combined to form ANFIS. The fuzzy technique incorporates "If-Then" rules created by specialists based on their knowledge and the system's provided database [7]. It can function in uncertain systems. But learning is the fundamental flaw in the fuzzy approach [8]. Alternatively, meanwhile, the neural network approach has the capacity to learn, but it lacks the power to provide decisions. ANFIS helps to optimize gains while minimizing error. ANFIS has incorporated the beneficial aspects of fuzzy and neural techniques.

The back-propagation and hybrid learning algorithms are the two types of algorithms used in ANFIS. For parameter optimization, the back-propagation algorithm is in use [9]. The membership functions for the fuzzy method are trained using the hybrid learning technique.

ANFIS Structure employs learning supervision for learning algorithms and performs a similar role to the Sugeno fuzzy model inference system. The Sugeno model for two inputs and one output is depicted in Figure 1, and its corresponding ANFIS Structure is clarified in Figure 2. The rules in this situation will be:
Rule1: if (p) is (C_1) and (q) is (D_1) then ($r_1 = x_1p + y_1q + z_1$).
Rule2: if (p) is (C_2) and (q) is (D_2) then ($r_2 = x_2p + y_2q + z_2$).

where (p,q) are crisp inputs. (x_i,y_i,z_i) are the parameters identified by the training process. (C_i,D_i) are fuzzy sets.

As depicted in Figure 2, the ANFIS structure is comprised of five layers [7, 8]. Hereunder is a quick summary of each layer:

Layer1: This layer has adaptable nodes with the following membership functions:

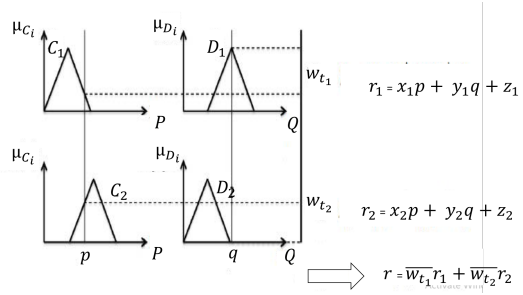

Figure 1. Sugeno system.

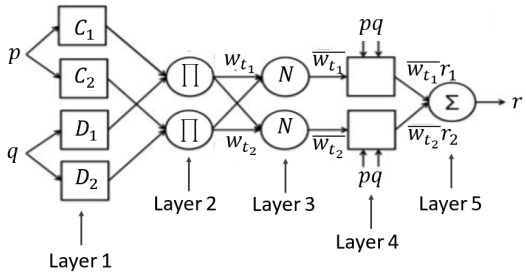

Figure 2. ANFIS structure.

$$\begin{aligned} O_i^1 &= \mu_{C_i}(p) \qquad i = 1,2, \\ O_i^1 &= \mu_{D_i}(q) \qquad i = 1,2. \end{aligned} \tag{4}$$

Layer 2: It determines a rule's firing strength in accordance with (5)

$$O_i^2 = w_{ti} = \mu_{C_i}(p) \times \mu_{D_i}(q) \qquad i = 1,2. \tag{5}$$

Layer 3: This layer calculates the normalization of a rule's firing strength.

$$O_i^3 = \overline{w_{ti}} = \frac{w_{ti}}{w_{t1} + w_{t2}} \qquad i = 1,2. \tag{6}$$

Layer 4: Each node in this layer represents consequent part of fuzzy rule. The square node encompasses a linear function of the inputs such as:

$$O_i^4 = \overline{w_{ti}} r_i = \overline{w_{ti}}(x_i p + y_i q + z_i). \tag{7}$$

Layer 5: All incoming signals are summed at this layer as in (8)

$$O_i^5 = \sum_i \overline{w_{ti}} r_i. \tag{8}$$

4. ANFIS based controller design

The discrepancy between the current attitude $\boldsymbol{\eta} = \begin{bmatrix} \eta_1 & \eta_2 & \eta_3 & \eta_4 \end{bmatrix}^T$ and the desired attitude $\boldsymbol{\eta_t} = \begin{bmatrix} \eta_{1c} & \eta_{2c} & \eta_{3c} & \eta_{4c} \end{bmatrix}^T$ is expressed by the attitude error vector $\boldsymbol{\mu_e} = \begin{bmatrix} \mu_{e_1} & \mu_{e_2} & \mu_{e_3} \end{bmatrix}^T$. As in [10], this vector is computed as

$$\boldsymbol{\mu_e} = 2\eta_{4e} \begin{bmatrix} \eta_{1e} & \eta_{2e} & \eta_{3e} \end{bmatrix}^T, \tag{9}$$

where $\begin{bmatrix} \eta_{4e} \\ \eta_{1e} \\ \eta_{2e} \\ \eta_{3e} \end{bmatrix} = \begin{bmatrix} \eta_{4c} & \eta_{1c} & \eta_{2c} & \eta_{3c} \\ -\eta_{1c} & \eta_{4c} & \eta_{3c} & -\eta_{2c} \\ -\eta_{2c} & -\eta_{3c} & \eta_{4c} & \eta_{1c} \\ -\eta_{3c} & \eta_{2c} & -\eta_{1c} & \eta_{4c} \end{bmatrix} \begin{bmatrix} \eta_4 \\ \eta_1 \\ \eta_2 \\ \eta_3 \end{bmatrix}$.

For attitude loops, this design uses 49 fuzzy rules and seven membership functions of triangular shape, as depicted in Figure 3 to Figure 8.

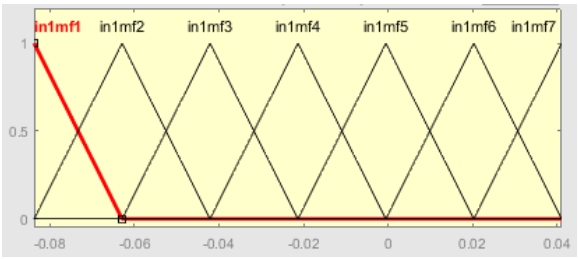

Figure 3. First element of the attitude error vector Membership function.

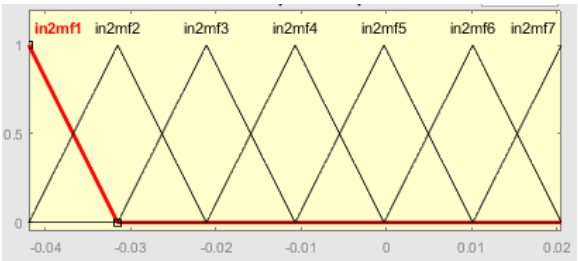

Figure 4. Change of first element of the attitude error vector Membership function.

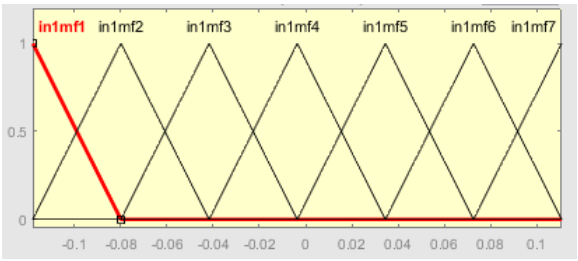

Figure 5. Second element of the attitude error vector Membership function.

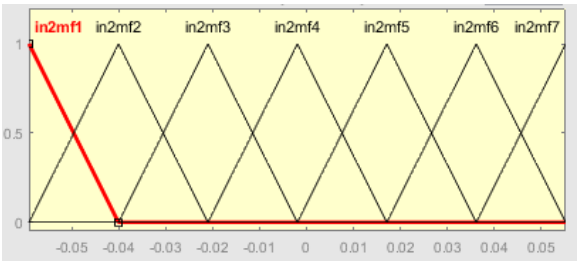

Figure 6. Change of second element of the attitude error vector Membership function.

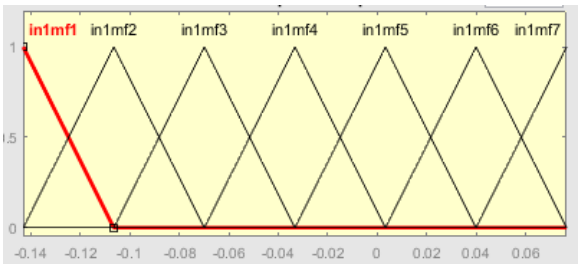

Figure 7. Third element of the attitude error vector Membership function.

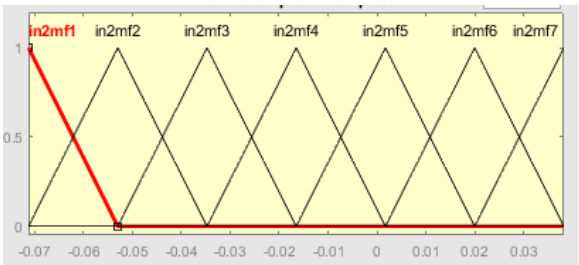

Figure 8. Change of third element of the attitude error vector Membership function.

5. Simulation and analysis

This section illustrates the designed flight controller's robustness and efficiency by comparing the designed intelligent adaptive controller and the GA-adjusted PD and LQR controllers presented in [3].

For the ACS, nominal mode post detumbling was addressed. The simulation time has been split into two periods. The ACS's effectiveness in stabilization is measured during the first 100-second period. One degree per second was used as the starting satellite angular rate. The referenced Euler angles are (roll, pitch, and yaw) [*deg*], (0,0,0). Euler angles will be employed to indicate the orientation of the satellite rather than quaternions for simplicity of visualization. The effectiveness of the ACS in reorienting the satellite is measured in the second interval. This span of time is split into four 100-second segments. The commanded attitude angles, in this case, are as follows: (-25,20,-40), (25,-20,40), (65,40,60), and (20,60,5) [*deg*].

5.1. Analysis without including uncertainties

The comparison of the aforementioned controllers without uncertainties and actuator toque noise is covered in this subsection. Only disruptive torques caused by the space environment are considered in this scenario.

Considering the simulation outcomes shown in Figures 9-10, and Table 1, the performance of ANFIS-based ACS is in equal standing with that of GA PD ACS. Still, it outperforms LQR since it ensures quicker stabilization, quicker settling response, and lower pointing errors. Moreover, The proposed controller performs more robustly than the LQR flight controller. It can successfully overcome and reject environmental disturbances. Despite all these advantages the proposed controller requires slightly higher torque.

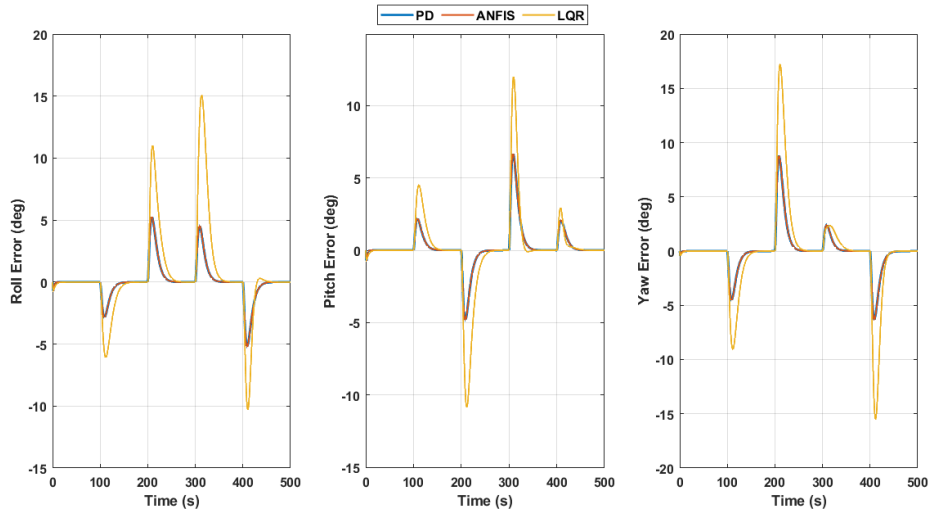

Figure 9. Attitude error.

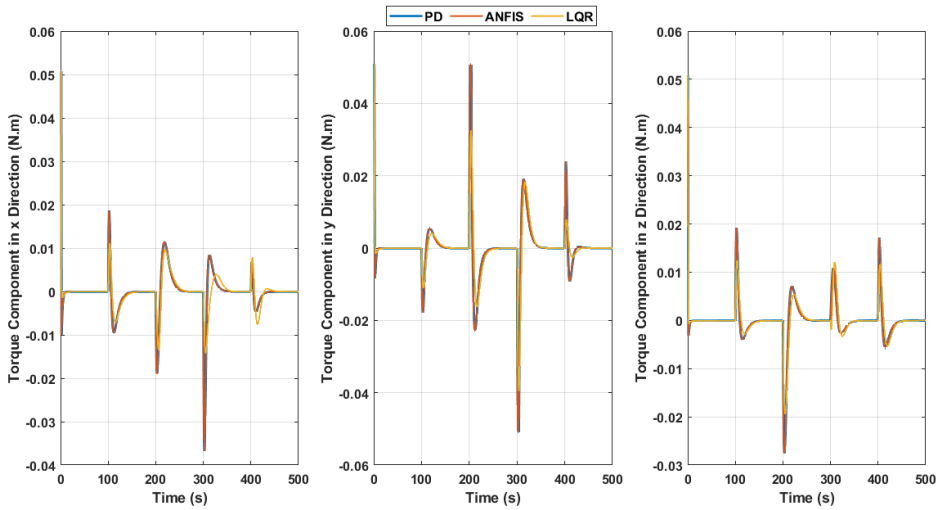

Figure 10. Actuators torque.

Table 1. Performance comparison before adding uncertainties.

Euler Angle	Controller	Stabilization		Reorientation	
		Time for Stabilization [s]	Pointing Error [deg]	Settling Time [s]	Pointing Error [deg]
Roll Angle	ANFIS	<12	<0.00012	<51	<0.0011
	GA PD [3]	<11	<0.0001	<50	<0.001
	LQR [3]	<16	<0.0015	<65	<0.003
Pitch Angle	ANFIS	<10	<0.00053	<42	<0.0021
	GA PD [3]	<10	<0.0005	<40	<0.002
	LQR [3]	<15	<0.0015	<50	<0.009
Yaw Angle	ANFIS	<8	<0.00031	<56	<0.0011
	GA PD [3]	<8	<0.0003	<55	<0.001
	LQR [3]	<12	<0.0015	<60	<0.003

5.2. Uncertainties effect

The comparison is carried out in this subsection while considering satellite mathematical modeling uncertainties clarified in Table 2, besides actuator torque noise and environmentally disturbing torques. An additive actuator noise torque corresponding to 20 % of the controlling torque is constructed. This torque is modeled in the form of white noise. The instantaneous ratio of this torque is developed using a uniformly distributed random variable that varies between {-r,r}, where r is equal to 0.2.

The simulation results in Figure 11 and Table 3 clarify that ANFIS-based ACS provides for stabilization task a pointing error <0.045 [*deg*] compared to a value <0.15 [*deg*] obtained by the LQR flight controller, whereas a pointing accuracy <0.12 [*deg*] has been achieved using ANFIS ACS for reorientation maneuvers, which is less than one-half the value obtained using LQR control technique. Moreover, the LQR controller cannot surpass the fast response of the ANFIS-based and PD-based flight controllers. The expense of this is the additional torque needed, as depicted in Figure 12. Finally, the presented ACS could accomplish the performance of the pointing requirements (<0.3 [*deg*]).

Table 2. Satellite parametric uncertainties.

Parameter	Uncertainty (%)
Satellite moment of inertia	25
Reaction wheel's moment of inertia	25
Satellite center of mass	25

Table 3. Performance comparison after adding uncertainties.

Euler Angle	Controller	Stabilization		Reorientation	
		Time for Stabilization [s]	Pointing Error [deg]	Settling Time [s]	Pointing Error [deg]
Roll Angle	ANFIS	<12	<0.013	<51	<0.052
	GA PD [3]	<11	<0.01	<50	<0.05
	LQR [3]	<16	<0.07	<65	<0.2
Pitch Angle	ANFIS	<10	<0.035	<42	<0.051
	GA PD [3]	<10	<0.03	<40	<0.05
	LQR [3]	<15	<0.07	<50	<0.15
Yaw Angle	ANFIS	<8	<0.022	<56	<0.082
	GA PD [3]	<8	<0.02	<55	<0.08
	LQR [3]	<12	<0.07	<60	<0.2

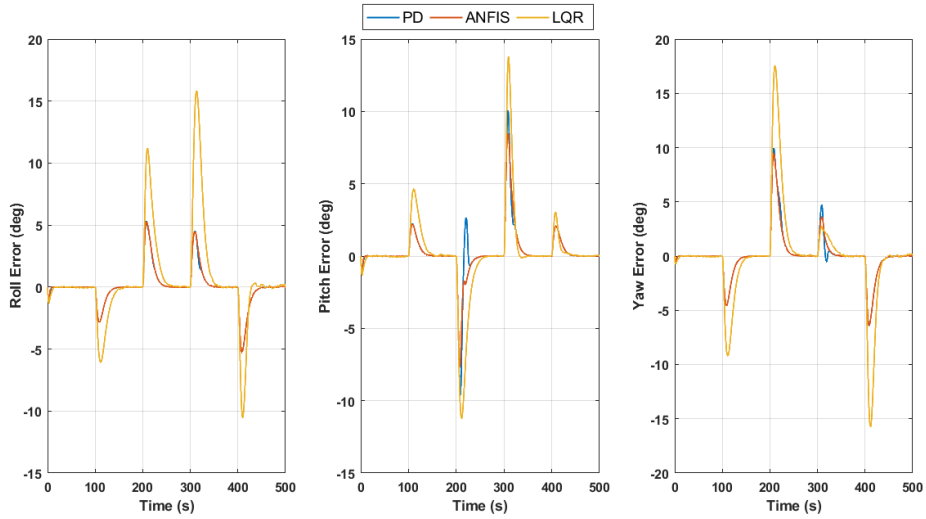

Figure 11. Attitude error.

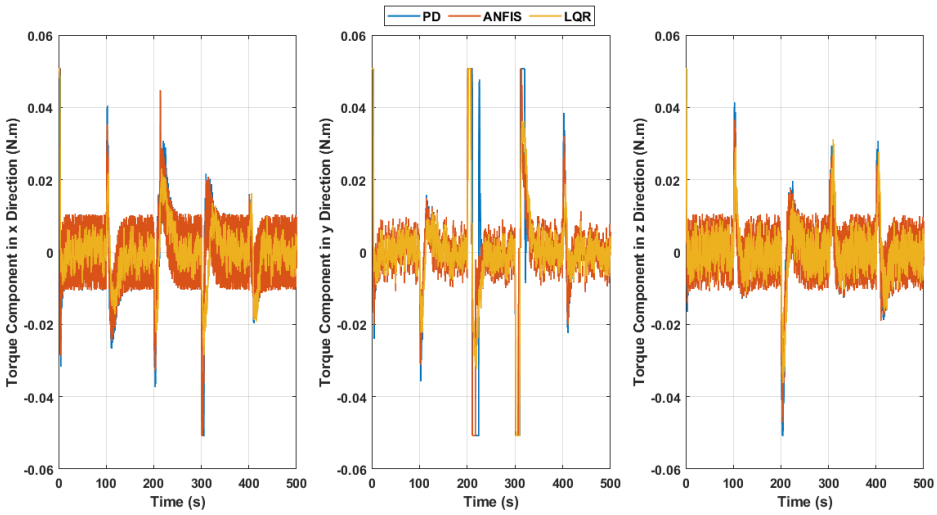

Figure 12. Actuators torque.

6. Conclusion

In this study, a reliable adaptive flight controller for satellite ACS is constructed. This controller is an ANFIS-based intelligent flight controller. The simulation results indicate that when the satellite is subjected to environmental disturbances, the developed controller performs roughly similar to the GA PD controller in [3]. However, the offered controller outperformed the LQR controller developed in [3] in terms of performance. Furthermore, when dealing with torque noise induced by actuator vibrations and the satellite's parametric uncertainty, the ACS based on the suggested ANFIS performs exceptionally well.

References

[1] Narkiewicz J, Sochacki M and Zakrzewski B 2020 Generic model of a satellite attitude control system *Int. J. of Aerospace Engineering* **2020**

[2] De Ruiter AH, Damaren C and Forbes JR 2012 *Spacecraft Dynamics and Control: an Introduction* (New Jersey, USA: John Wiley & Sons)
[3] Elrouby A, Hendy H and Ashry M 2022 Comparative analysis of attitude control systems for small satellites based on linear controllers *18th Int. Computer Engineering Conf.* vol 1 pp 97–101
[4] Elrouby A, Hendy H and Ashry M 2022 Robust performance attitude control system for nano-satellites *13th Int. Conf. on Elec. Eng.* pp 27–31
[5] Omar S 2015 An inverse dynamics satellite attitude determination and control system with autonomous calibration *29th Annual AIAA/USU Conf. on Small Satellites*
[6] Ismail Z and Varatharajoo R 2010 A study of reaction wheel configurations for a 3-axis satellite attitude control *Advances in Space Research* **45**(6) pp 750–759
[7] Kar S, Das S and Ghosh PK 2014 Applications of neuro fuzzy systems: A brief review and future outline *Applied Soft Computing* **15** pp 243–259
[8] Joshi N and Jharia B 2015 Optimized fuzzy power control over fading channels in spectrum sharing cognitive radio using ANFIS *2nd Int. Conf. on Signal Processing and Integrated Networks* pp 329–333
[9] Chen X and Zhang X 2015 Nonlinear feedback control based on ANFIS *12th Int. Conf. on Fuzzy Systems and Knowledge Discovery* pp 559–563
[10] Sidi MJ 1997 *Spacecraft Dynamics and Control: a Practical Engineering Approach* vol 7 (New York, USA: Cambridge University Press)